A direct measurement of the W boson decay width

V.M. Abazov,[23] B. Abbott,[57] A. Abdesselam,[11] M. Abolins,[50] V. Abramov,[26] B.S. Acharya,[17] D.L. Adams,[55] M. Adams,[37] S.N. Ahmed,[21] G.D. Alexeev,[23] A. Alton,[49] G.A. Alves,[2] E.W. Anderson,[42] Y. Arnoud,[9] C. Avila,[5] M.M. Baarmand,[54] V.V. Babintsev,[26] L. Babukhadia,[54] T.C. Bacon,[28] A. Baden,[46] B. Baldin,[36] P.W. Balm,[20] S. Banerjee,[17] E. Barberis,[30] P. Baringer,[43] J. Barreto,[2] J.F. Bartlett,[36] U. Bassler,[12] D. Bauer,[28] A. Bean,[43] F. Beaudette,[11] M. Begel,[53] A. Belyaev,[35] S.B. Beri,[15] G. Bernardi,[12] I. Bertram,[27] A. Besson,[9] R. Beuselinck,[28] V.A. Bezzubov,[26] P.C. Bhat,[36] V. Bhatnagar,[15] M. Bhattacharjee,[54] G. Blazey,[38] F. Blekman,[20] S. Blessing,[35] A. Boehnlein,[36] N.I. Bojko,[26] T.A. Bolton,[44] F. Borcherding,[36] K. Bos,[20] T. Bose,[52] A. Brandt,[59] R. Breedon,[31] G. Briskin,[58] R. Brock,[50] G. Brooijmans,[36] A. Bross,[36] D. Buchholz,[39] M. Buehler,[37] V. Buescher,[14] V.S. Burtovoi,[26] J.M. Butler,[47] F. Canelli,[53] W. Carvalho,[3] D. Casey,[50] Z. Casilum,[54] H. Castilla-Valdez,[19] D. Chakraborty,[38] K.M. Chan,[53] S.V. Chekulaev,[26] D.K. Cho,[53] S. Choi,[34] S. Chopra,[55] J.H. Christenson,[36] M. Chung,[37] D. Claes,[51] A.R. Clark,[30] L. Coney,[41] B. Connolly,[35] W.E. Cooper,[36] D. Coppage,[43] S. Crépé-Renaudin,[9] M.A.C. Cummings,[38] D. Cutts,[58] G.A. Davis,[53] K. De,[59] S.J. de Jong,[21] M. Demarteau,[36] R. Demina,[44] P. Demine,[9] D. Denisov,[36] S.P. Denisov,[26] S. Desai,[54] H.T. Diehl,[36] M. Diesburg,[36] S. Doulas,[48] Y. Ducros,[13] L.V. Dudko,[25] S. Duensing,[21] L. Duflot,[11] S.R. Dugad,[17] A. Duperrin,[10] A. Dyshkant,[38] D. Edmunds,[50] J. Ellison,[34] J.T. Eltzroth,[59] V.D. Elvira,[36] R. Engelmann,[54] S. Eno,[46] G. Eppley,[61] P. Ermolov,[25] O.V. Eroshin,[26] J. Estrada,[53] H. Evans,[52] V.N. Evdokimov,[26] T. Fahland,[33] D. Fein,[29] T. Ferbel,[53] F. Filthaut,[21] H.E. Fisk,[36] Y. Fisyak,[55] E. Flattum,[36] F. Fleuret,[12] M. Fortner,[38] H. Fox,[39] K.C. Frame,[50] S. Fu,[52] S. Fuess,[36] E. Gallas,[36] A.N. Galyaev,[26] M. Gao,[52] V. Gavrilov,[24] R.J. Genik II,[27] K. Genser,[36] C.E. Gerber,[37] Y. Gershtein,[58] R. Gilmartin,[35] G. Ginther,[53] B. Gómez,[5] P.I. Goncharov,[26] H. Gordon,[55] L.T. Goss,[60] K. Gounder,[36] A. Goussiou,[28] N. Graf,[55] P.D. Grannis,[54] J.A. Green,[42] H. Greenlee,[36] Z.D. Greenwood,[45] S. Grinstein,[1] L. Groer,[52] S. Grünendahl,[36] A. Gupta,[17] S.N. Gurzhiev,[26] G. Gutierrez,[36] P. Gutierrez,[57] N.J. Hadley,[46] H. Haggerty,[36] S. Hagopian,[35] V. Hagopian,[35] R.E. Hall,[32] S. Hansen,[36] J.M. Hauptman,[42] C. Hays,[52] C. Hebert,[43] D. Hedin,[38] J.M. Heinmiller,[37] A.P. Heinson,[34] U. Heintz,[47] M.D. Hildreth,[41] R. Hirosky,[62] J.D. Hobbs,[54] B. Hoeneisen,[8] Y. Huang,[49] I. Iashvili,[34] R. Illingworth,[28] A.S. Ito,[36] M. Jaffré,[11] S. Jain,[17] R. Jesik,[28] K. Johns,[29] M. Johnson,[36] A. Jonckheere,[36] H. Jöstlein,[36] A. Juste,[36] W. Kahl,[44] S. Kahn,[55] E. Kajfasz,[10] A.M. Kalinin,[23] D. Karmanov,[25] D. Karmgard,[41] R. Kehoe,[50] A. Khanov,[44] A. Kharchilava,[41] S.K. Kim,[18] B. Klima,[36] B. Knuteson,[30] W. Ko,[31] J.M. Kohli,[15] A.V. Kostritskiy,[26] J. Kotcher,[55] B. Kothari,[52] A.V. Kotwal,[52] A.V. Kozelov,[26] E.A. Kozlovsky,[26] J. Krane,[42] M.R. Krishnaswamy,[17] P. Krivkova,[6] S. Krzywdzinski,[36] M. Kubantsev,[44] S. Kuleshov,[24] Y. Kulik,[36] S. Kunori,[46] A. Kupco,[7] V.E. Kuznetsov,[34] G. Landsberg,[58] W.M. Lee,[35] A. Leflat,[25] C. Leggett,[30] F. Lehner,[36,*] C. Leonidopoulos,[52] J. Li,[59] Q.Z. Li,[36] J.G.R. Lima,[3] D. Lincoln,[36] S.L. Linn,[35] J. Linnemann,[50] R. Lipton,[36] A. Lucotte,[9] L. Lueking,[36] C. Lundstedt,[51] C. Luo,[40] A.K.A. Maciel,[38] R.J. Madaras,[30] V.L. Malyshev,[23] V. Manankov,[25] H.S. Mao,[4] T. Marshall,[40] M.I. Martin,[38] A.A. Mayorov,[26] R. McCarthy,[54] T. McMahon,[56] H.L. Melanson,[36] M. Merkin,[25] K.W. Merritt,[36] C. Miao,[58] H. Miettinen,[61] D. Mihalcea,[38] C.S. Mishra,[36] N. Mokhov,[36] N.K. Mondal,[17] H.E. Montgomery,[36] R.W. Moore,[50] M. Mostafa,[1] H. da Motta,[2] Y. Mutaf,[54] E. Nagy,[10] F. Nang,[29] M. Narain,[47] V.S. Narasimham,[17] N.A. Naumann,[21] H.A. Neal,[49] J.P. Negret,[5] A. Nomerotski,[36] T. Nunnemann,[36] D. O'Neil,[50] V. Oguri,[3] B. Olivier,[12] N. Oshima,[36] P. Padley,[61] L.J. Pan,[39] K. Papageorgiou,[37] N. Parashar,[48] R. Partridge,[58] N. Parua,[54] M. Paterno,[53] A. Patwa,[54] B. Pawlik,[22] O. Peters,[20] P. Pétroff,[11] R. Piegaia,[1] B.G. Pope,[50] E. Popkov,[47] H.B. Prosper,[35] S. Protopopescu,[55] M.B. Przybycien,[39,†] J. Qian,[49] R. Raja,[36] S. Rajagopalan,[55] E. Ramberg,[36] P.A. Rapidis,[36] N.W. Reay,[44] S. Reucroft,[48] M. Ridel,[11] M. Rijssenbeek,[54] F. Rizatdinova,[44] T. Rockwell,[50] M. Roco,[36] C. Royon,[13] P. Rubinov,[36] R. Ruchti,[41] J. Rutherfoord,[29] B.M. Sabirov,[23] G. Sajot,[9] A. Santoro,[3] L. Sawyer,[45] R.D. Schamberger,[54] H. Schellman,[39] A. Schwartzman,[1] N. Sen,[61] E. Shabalina,[37] R.K. Shivpuri,[16] D. Shpakov,[48] M. Shupe,[29] R.A. Sidwell,[44] V. Simak,[7] H. Singh,[34] V. Sirotenko,[36] P. Slattery,[53] E. Smith,[57] R.P. Smith,[36] R. Snihur,[39] G.R. Snow,[51] J. Snow,[56] S. Snyder,[55] J. Solomon,[37] Y. Song,[59] V. Sorín,[1] M. Sosebee,[59] N. Sotnikova,[25] K. Soustruznik,[6] M. Souza,[2] N.R. Stanton,[44] G. Steinbrück,[52] R.W. Stephens,[59] D. Stoker,[33] V. Stolin,[24] A. Stone,[45] D.A. Stoyanova,[26] M.A. Strang,[59] M. Strauss,[57] M. Strovink,[30] L. Stutte,[36] A. Sznajder,[3] M. Talby,[10] W. Taylor,[54] S. Tentindo-Repond,[35] S.M. Tripathi,[31] T.G. Trippe,[30] A.S. Turcot,[55] P.M. Tuts,[52] V. Vaniev,[26] R. Van Kooten,[40] N. Varelas,[37] L.S. Vertogradov,[23] F. Villeneuve-Seguier,[10] A.A. Volkov,[26] A.P. Vorobiev,[26] H.D. Wahl,[35] H. Wang,[39] Z.-M. Wang,[54] J. Warchol,[41] G. Watts,[63] M. Wayne,[41] H. Weerts,[50] A. White,[59] J.T. White,[60] D. Whiteson,[30] D.A. Wijngaarden,[21] S. Willis,[38] S.J. Wimpenny,[34] J. Womersley,[36] D.R. Wood,[48] Q. Xu,[49] R. Yamada,[36] P. Yamin,[55] T. Yasuda,[36] Y.A. Yatsunenko,[23] K. Yip,[55] S. Youssef,[35] J. Yu,[59] M. Zanabria,[5] X. Zhang,[57] H. Zheng,[41] B. Zhou,[49] Z. Zhou,[42]

M. Zielinski,[53] D. Zieminska,[40] A. Zieminski,[40] V. Zutshi,[38] E.G. Zverev,[25] and A. Zylberstejn[13]

(DØ Collaboration)

[1] *Universidad de Buenos Aires, Buenos Aires, Argentina*
[2] *LAFEX, Centro Brasileiro de Pesquisas Físicas, Rio de Janeiro, Brazil*
[3] *Universidade do Estado do Rio de Janeiro, Rio de Janeiro, Brazil*
[4] *Institute of High Energy Physics, Beijing, People's Republic of China*
[5] *Universidad de los Andes, Bogotá, Colombia*
[6] *Charles University, Center for Particle Physics, Prague, Czech Republic*
[7] *Institute of Physics, Academy of Sciences, Center for Particle Physics, Prague, Czech Republic*
[8] *Universidad San Francisco de Quito, Quito, Ecuador*
[9] *Institut des Sciences Nucléaires, IN2P3-CNRS, Universite de Grenoble 1, Grenoble, France*
[10] *CPPM, IN2P3-CNRS, Université de la Méditerranée, Marseille, France*
[11] *Laboratoire de l'Accélérateur Linéaire, IN2P3-CNRS, Orsay, France*
[12] *LPNHE, Universités Paris VI and VII, IN2P3-CNRS, Paris, France*
[13] *DAPNIA/Service de Physique des Particules, CEA, Saclay, France*
[14] *Universität Mainz, Institut für Physik, Mainz, Germany*
[15] *Panjab University, Chandigarh, India*
[16] *Delhi University, Delhi, India*
[17] *Tata Institute of Fundamental Research, Mumbai, India*
[18] *Seoul National University, Seoul, Korea*
[19] *CINVESTAV, Mexico City, Mexico*
[20] *FOM-Institute NIKHEF and University of Amsterdam/NIKHEF, Amsterdam, The Netherlands*
[21] *University of Nijmegen/NIKHEF, Nijmegen, The Netherlands*
[22] *Institute of Nuclear Physics, Kraków, Poland*
[23] *Joint Institute for Nuclear Research, Dubna, Russia*
[24] *Institute for Theoretical and Experimental Physics, Moscow, Russia*
[25] *Moscow State University, Moscow, Russia*
[26] *Institute for High Energy Physics, Protvino, Russia*
[27] *Lancaster University, Lancaster, United Kingdom*
[28] *Imperial College, London, United Kingdom*
[29] *University of Arizona, Tucson, Arizona 85721*
[30] *Lawrence Berkeley National Laboratory and University of California, Berkeley, California 94720*
[31] *University of California, Davis, California 95616*
[32] *California State University, Fresno, California 93740*
[33] *University of California, Irvine, California 92697*
[34] *University of California, Riverside, California 92521*
[35] *Florida State University, Tallahassee, Florida 32306*
[36] *Fermi National Accelerator Laboratory, Batavia, Illinois 60510*
[37] *University of Illinois at Chicago, Chicago, Illinois 60607*
[38] *Northern Illinois University, DeKalb, Illinois 60115*
[39] *Northwestern University, Evanston, Illinois 60208*
[40] *Indiana University, Bloomington, Indiana 47405*
[41] *University of Notre Dame, Notre Dame, Indiana 46556*
[42] *Iowa State University, Ames, Iowa 50011*
[43] *University of Kansas, Lawrence, Kansas 66045*
[44] *Kansas State University, Manhattan, Kansas 66506*
[45] *Louisiana Tech University, Ruston, Louisiana 71272*
[46] *University of Maryland, College Park, Maryland 20742*
[47] *Boston University, Boston, Massachusetts 02215*
[48] *Northeastern University, Boston, Massachusetts 02115*
[49] *University of Michigan, Ann Arbor, Michigan 48109*
[50] *Michigan State University, East Lansing, Michigan 48824*
[51] *University of Nebraska, Lincoln, Nebraska 68588*
[52] *Columbia University, New York, New York 10027*
[53] *University of Rochester, Rochester, New York 14627*
[54] *State University of New York, Stony Brook, New York 11794*
[55] *Brookhaven National Laboratory, Upton, New York 11973*
[56] *Langston University, Langston, Oklahoma 73050*
[57] *University of Oklahoma, Norman, Oklahoma 73019*

[58] *Brown University, Providence, Rhode Island 02912*
[59] *University of Texas, Arlington, Texas 76019*
[60] *Texas A&M University, College Station, Texas 77843*
[61] *Rice University, Houston, Texas 77005*
[62] *University of Virginia, Charlottesville, Virginia 22901*
[63] *University of Washington, Seattle, Washington 98195*

Based on 85 pb^{-1} data of $p\overline{p}$ collisions at $\sqrt{s} = 1.8$ TeV collected using the DØ detector at Fermilab during the 1994-1995 run of the Tevatron, we present a direct measurement of the total decay width of the W boson, Γ_W. The width is determined from the transverse mass spectrum in the $W \to e + \nu_e$ decay channel and found to be $\Gamma_W = 2.23^{+0.15}_{-0.14}$(stat.)$\pm$0.10(syst.)GeV, consistent with the expectation from the standard model.

March 30, 2002

I. INTRODUCTION

The theory that describes the fundamental particle interactions is called the standard model (SM). The standard model is a gauge field theory that comprises the Glashow-Weinberg-Salam (GWS) model [1–3] of the weak and electromagnetic interactions and quantum chromodynamics (QCD) [4–6], the theory of the strong interactions. The discovery of the W [7,8] and Z [9,10] bosons in 1983 by the UA1 and UA2 collaborations at the CERN $p\overline{p}$ collider provided a direct confirmation of the unification of the weak and electromagnetic interactions. Experiments have been refining the measurements of the characteristics of the W and Z bosons. The total decay width of W boson, Γ_W, is given in the SM in terms of the masses of the gauge bosons and their couplings to their decay products.

In $p\overline{p}$ collisions, W bosons are produced by processes of the type $u\overline{d}$ or $\overline{u}d \to W$, followed by subsequent leptonic or hadronic decay: $W \to \ell\nu$ or $W \to q'\overline{q}$, where $\ell = e, \mu, \tau$, and q' or q represent one of the quarks u, d, c, s or b (but not t since top quark is heavier than the W boson).

At lowest order in perturbation theory, the SM predicts the partial decay width $\Gamma(W \to e\nu)$ of $W \to e\nu$ to be $\Gamma(W \to e\nu) = g^2 M_W/48\pi$ [11]. Including radiative corrections, this can be rewritten as:

$$\Gamma(W \to e\nu) = \frac{G_F M_W^3}{6\sqrt{2}\pi}(1 + \delta_{\rm SM}). \qquad (1)$$

where $G_F/\sqrt{2} = g^2/8M_W^2$, g is the charged current coupling, and M_W is the mass of the W boson. The SM radiative correction, $\delta_{\rm SM}$, is calculated [12] to be less than $\frac{1}{2}$%. By using the experimental values of G_F (measured from muon decay [13]) and M_W (measured at the Fermilab Tevatron collider [14,15] and LEP2 [16–19]), the predicted partial width is [11] $\Gamma(W \to e\nu) = 226.5 \pm 0.3$ MeV

A W boson has three leptonic decay channels and two dominant hadronic decay channels, $W \to e\bar{\nu}, \mu\bar{\nu}, \tau\bar{\nu}$ and qq', where q is u or c, and q' is the appropriate CKM mixture of d and s. Other hadronic decay channels are greatly suppressed by CKM off-diagonal matrix elements. Considering the three color charges for quarks, these nine leptonic and hadronic channels yield a total width of $\approx 9\Gamma(W \to e\nu)$. Including QCD corrections, the leptonic decay branching ratio is $B(W \to e\nu) = 1/\{3 + 6[1 + \alpha_s(M_W)/\pi + \mathcal{O}(\alpha_s^2)]\}$, leading to the SM prediction for the full width of the W boson [11] of $\Gamma_W = 2.0921 \pm 0.0025$ GeV.

Historically, the accurate determination of the width of the W boson was available through an indirect measurement using the ratio $\mathcal{R}$ of the $W \to e\nu$ and $Z \to ee$ cross sections:

$$\mathcal{R} = \frac{\sigma(p\bar{p} \to W + X) \cdot Br(W \to e\nu)}{\sigma(p\bar{p} \to Z + X) \cdot Br(Z \to ee)} = \frac{\sigma_W}{\sigma_Z} \cdot \frac{Br(W \to e\nu)}{Br(Z \to ee)}. \qquad (2)$$

A measurement of $\mathcal{R}$, together with a calculation [20] of the ratio of production cross sections σ_W/σ_Z and the measurement of the branching faction $Br(Z \to ee) = \Gamma(Z \to ee)/\Gamma(Z)$ from the CERN e^+e^- collider (LEP) [21], can be used to extract the W boson leptonic branching ratio $Br(W \to e\nu) = \Gamma(W \to e\nu)/\Gamma(W)$, which, in turn, yields the full width of the W boson from calculated partial decay width $\Gamma(W \to e\nu)$. Thus, in this indirect measurement, calculations of σ_W/σ_Z and the partial width $\Gamma(W \to e\nu)$ yield Γ_W in the context of the SM. This method was first used by the UA1 [22] and UA2 [23] collaborations. More recently, the CDF [24] and DØ [25] collaborations obtained $\Gamma_W = 2.064 \pm 0.084$ GeV and $\Gamma_W = 2.169 \pm 0.079$ GeV, respectively, using this technique.

The value of Γ_W can also be obtained from the line shape of the transverse mass m_T of the W boson, because the Breit-Wigner (width) component of the line shape falls off more slowly at high m_T than the resolution component does [12]. The transverse mass is given by

$$m_T = \sqrt{2E_T^e E_T^\nu[1 - \cos(\phi^e - \phi^\nu)]} \qquad (3)$$

where E_T^e and E_T^ν are the transverse energies, and ϕ^e and ϕ^ν are the azimuthal angles, of the electron and neutrino, respectively. The transverse mass has a kinematic upper limit at the value of M_W, and the shape of the m_T distribution at this upper limit, called the "Jacobian edge," is sensitive to Γ_W [26]. Using this technique, the CDF collaboration reported [27] a measurement of $\Gamma_W = 2.05 \pm 0.10$(stat.)± 0.08(syst.) GeV. Figure 1 shows the m_T spectrum shape expected for different values of Γ_W and indicates the sensitivity of the tail of the transverse mass distribution to Γ_W. Clearly, the effect is greatest in the region above m_W.

The direct measurement of Γ_W complements the indirect measurement through $\mathcal{R}$ in several ways:

- Theoretical inputs for σ_W/σ_Z and $\Gamma(W \to e\nu)$, which may be sensitive to non-SM coupling of the W boson, are not needed.

- The direct measurement explores the region above the W boson mass pole, where possible new phenomena such as an additional heavy vector boson (W') can contribute.

- It is desirable to have more than one method of measuring a given property. The sources of systematic errors in the two methods are

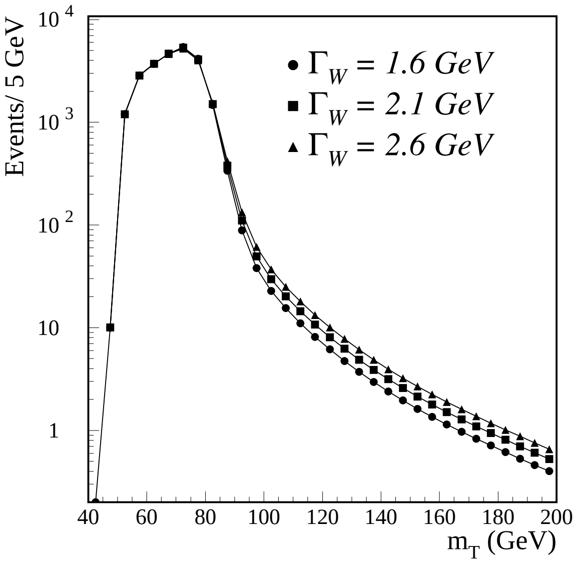

FIG. 1. Monte Carlo simulations of the transverse mass spectrum for different W boson widths. The selections, $E_T(e) > 25$ GeV and $E_T(\nu) > 25$ GeV, are applied to MC sample. The circles show the spectrum for $\Gamma_W = 1.60$ GeV, the squares for $\Gamma_W = 2.10$ GeV, and triangles for $\Gamma_W = 2.60$ GeV. Distribution are normalized arbitrarily in the transverse mass region shown.

different, and the direct method will be important when the measurement through $\mathcal{R}$ becomes limited by systematic uncertainty.

The paper is organized as follows. In Sec. II, we give a brief description of the DØ detector. Particle identification and event selection are discussed in Sec. III. The analysis procedure, including background estimation and Monte Carlo simulation, is described in Sec. IV, and the conclusions are presented in Sec. V. For more detailed information on this analysis, see Ref. [28].

II. THE DØ DETECTOR

A. Experimental Apparatus

The DØ detector [30] comprises three major systems. The innermost of these is a non-magnetic tracker used in the reconstruction of charged particle tracks. The tracker is surrounded by central and forward uranium/liquid-argon sampling calorimeters. These calorimeters are used to identify electrons, photons, and hadronic jets, and to reconstruct their energies. The calorimeters are surrounded by a muon spectrometer used in the identification of muons and the reconstruction of their momenta. We use a coordinate system (ρ, θ, ϕ) where ρ is the perpendicular distance from the beam line, θ is the polar angle measured relative to the proton beam direction z, and ϕ is the azimuthal angle. The pseudorapidity η is defined as $-\ln(\tan\frac{\theta}{2})$. For this analysis, the relevant components are the tracking system and the calorimeters.

The central tracking system provides a measurement of the energy loss due to ionization (dE/dx) for tracks within its tracking volume. This information is used to help distinguish prompt electrons from e^+e^- pairs due to photon conversions.

The structure of the calorimeter has been optimized to distinguish electrons and photons from hadrons and to measure their energies. It is composed of three sections: the central calorimeter (CC), and two end calorimeters (EC). The η-coverage for electrons used in this analysis is $\mid \eta \mid < 1.1$ [29] in the CC region, which consists of 32 ϕ modules. The calorimeter is segmented longitudinally into three sections, the electromagnetic calorimeter (EM), the fine hadronic calorimeter (FH), and the coarse hadronic calorimeter (CH). The EM calorimeter is subdivided longitudinally into four layers (EM1–EM4). The first, second and fourth layers of the EM calorimeter are transversely divided into cells of size $\Delta\eta\times\Delta\phi = 0.1\times0.1$. The electromagnetic shower maximum occurs in the third layer, which is divided into finer units of 0.05×0.05 to improve the measurement of the shower shape and spatial resolution. There are 16 FH modules and 16 CH modules in ϕ. The fine hadronic calorimeter is subdivided longitudinally into three fine hadronic layers (FH1–FH3), and there is only one coarse hadronic layer.

B. Trigger

The DØ trigger has three levels, each applying increasingly more sophisticated selection criteria to an event. The lowest level trigger, Level 0, uses scintillation counters located on the inner faces of the forward calorimeters to signal the presence of an inelastic $p\overline{p}$ collision. Data from the Level 0 counters, the calorimeter, and the muon chambers are sent to the Level 1 trigger, which provides a trigger on total transverse energy (E_T), missing transverse energy $(\not\!\!E_T)$, E_T of individual calorimeter towers, and/or the presence of a muon. These triggers operate in less than 3.5 μs, the time between bunch crossings. Some calorimeter and muon-based triggers require additional time, which is provided by a Level 1.5 trigger system.

Level 1 (and 1.5) triggers initiate a Level 2 trigger system that consists of a farm of microprocessors. These microprocessors run simplified versions of the off-line event reconstruction algorithms to select events of interest.

III. PARTICLE IDENTIFICATION AND EVENT SELECTION

This analysis relies on the DØ detector's ability to identify electrons and to associate the undetected energy with neutrinos. We use both $W \to e\nu$ and $Z \to e^+e^-$ candidate samples for this analysis. The W boson candidate sample provides the signal events, while the $Z \to e^+e^-$ candidate sample is used to calibrate both the data and the Monte Carlo (MC) simulation. Candidate W and Z events are identified by the presence of an electron and a neutrino, or by the presence of two electrons with an invariant mass consistent with the mass of the Z boson, respectively. Electrons from W and Z boson decays typically have large transverse energy and are isolated from other particles. They are associated with a track in the tracking system and with a large deposit of energy in one of the EM calorimeters. Neutrinos do not interact in the detector, and thus create an apparent transverse energy imbalance in an event. For each W boson candidate event, we measure the energy imbalance in the plane transverse to the beam direction ($\not\!\!E_T$), and attribute this to the neutrino. The following sections provide a brief summary of the procedure [25] used in this analysis.

A. Electron Identification

Identification of electrons starts at the trigger level with the selection of clusters of electromagnetic energy. At Level 1, the trigger searches for EM calorimeter towers ($\Delta\phi \times \Delta\eta = 0.2 \times 0.2$) with signals that exceed predefined thresholds. W boson triggers require that the energy deposited in a single EM calorimeter tower exceed 10 GeV. Those events that satisfy the Level 1 trigger are processed by the Level 2 filter. The trigger towers are combined with the energy in the surrounding calorimeter cells within a window of $\Delta\phi \times \Delta\eta = 0.6 \times 0.6$.

Events are selected at Level 2 if the transverse energy in this window exceeds 20 GeV. In addition to the E_T requirement, the longitudinal and transverse shower shapes are required to match those expected for electromagnetic showers. The longitudinal shower shape is described by the fraction of the energy deposited in each of the four EM layers of the calorimeter. The transverse shower shape is characterized by energy deposition patterns in the third EM layer. The difference between the energies in concentric regions covering 0.25×0.25 and 0.15×0.15 in $\Delta\eta \times \Delta\phi$ must be consistent with that expected for an electron [30].

In addition, the electron candidates are required to deposit at least 90% of their energy in the EM section of the calorimeter and to be isolated from other calorimetric energy deposits. To be considered isolated, electrons must satisfy the isolation requirement, $f_{\rm iso} < 0.15$, where $f_{\rm iso}$ is defined as:

$$f_{\rm iso} = \frac{E_{\rm total}(0.4) - E_{\rm EM}(0.2)}{E_{\rm EM}(0.2)} \tag{4}$$

in which $E_{\rm total}(0.4)$ is the total energy, and $E_{\rm EM}(0.2)$ the electromagnetic energy, in cones of radius $R = \sqrt{(\Delta\eta)^2 + (\Delta\phi)^2} = 0.4$ and 0.2, respectively. This enhances the signal expected from isolated electrons in W and Z boson decay.

Having selected events with isolated electromagnetic showers at the trigger level, we first define "loose" electron for the purpose to study the background. Those EM clusters are require to locate within the center 80% of a calorimeter module, have an associated track in the central tracking volume and $|\eta| < 1.1$. To avoid areas of reduced response between neighboring calorimeter modules, the azimuthal angle of electrons is required to be at least $\Delta\phi = 0.10 \times 2\pi/32$ radians away from the position of a module boundary. We further impose a set of off-line tighter criteria to identify electrons, thereby reducing the background from QCD multijet events. The first step in identifying an electron is to form a cluster around the trigger tower using a nearest neighbor algorithm. As at the trigger level, the cluster is required to be isolated ($f_{\rm iso} < 0.15$). To increase the likelihood that the cluster is due to an electron and not a photon, a charged track from the central tracking system is required to point to the center of the EM cluster. We extrapolate the track to the third EM layer of the calorimeter and calculate the distance between the extrapolated track and the cluster centroid along the azimuthal direction ($\rho\Delta\phi$) and in the z-direction (Δz). The position of cluster centroid is defined at the radius of the third EM layer of the calorimeter. The z position of the event vertex is then defined by the line connecting the centroid position of the EM cluster to associated one in in the central tracking system and extrapolated to the beam line. The electron E_T is calculated using this vertex definition [25]. The variable

$$\sigma^2_{\rm trk} = \left(\frac{\rho\Delta\phi}{\sigma_{\rho\phi}}\right)^2 + \left(\frac{\Delta z}{\sigma_z}\right)^2. \tag{5}$$

where $\sigma_{\rho\phi}$ and σ_z are the respective track resolutions, quantifies the quality of the match. A requirement of $\sigma_{\rm trk} < 5$ is imposed on the data. These clusters are then subjected to a 4-variable likelihood test [31,32]. The four variables are:

- A χ^2 comparison of the shower shape with the expected shape of an electromagnetic shower, computed using a 41-variable covariance matrix [33] for the energy depositions in the cells of the electromagnetic calorimeter and the location of event vertex.

- The electromagnetic energy fraction, defined as the ratio of shower energy in the EM section of the calorimeter relative to the sum of EM energy plus the energy in the first hadronic section of the calorimeter.

- A comparison of the track position to the position of cluster centroid, as defined in Eq. 5.

- The ionization, dE/dx, along the track. This is used to reduce contamination due to e^+e^- pairs from photon conversions, mainly from jets fragmenting into neutral pions. The e^+e^- pair from photon conversion has a double value of dE/dx for a geniue electron due to two overlapping tracks,

To good approximation, these four variables are independent of each other for electron showers. Electrons that satisfy all above criteria are called "tight" electrons.

Electron energies are corrected for the underlying event energy that enter into the electron windows. The electromagnetic energy scale is determined in the test beam data, and adjusted to make the peak of the $Z \rightarrow e^+e^-$ invariant mass agree with the known mass of the Z boson [21]. We found it to be 0.9545 ± 0.0008. The electron energy scale is discussed in detail in Ref. [15].

B. Missing Transverse Energy

The primary sources of missing energy in an event include the neutrinos that pass through the calorimeter undetected and the calorimeter resolution. The energy imbalance is measured only in the transverse plane because of the lost particles emitted at small angles (within the beam pipes). The missing transverse energy is calculated by taking the negative of the vector sum of the transverse energy in all of the calorimeter cells. This gives both the magnitude and direction of $\not\!\!E_T$, allowing the calculation of the transverse mass of the W boson candidates.

C. Event Selection

The W boson data sample used in this analysis was collected during the 1994–1995 run of the Fermilab Tevatron collider, and corresponds to an integrated luminosity of 85.0 ± 3.6 pb^{-1}. Events are selected by requiring one tight electron in the central calorimeter ($|\ \eta\ | < 1.1$) [29] with $E_T > 25$ GeV. In addition, events are required to have $\not\!\!E_T > 25$ GeV and W transverse momentum $p_T(W) < 15$ GeV, which is combined transverse momentum of electron and $\not\!\!E_T$ (neutrino). After applying all of the described selections, a total of 24487 W boson candidates is selected. There are 24479 candidates in the region 0 - 200 GeV, while 8(2) candidates have m_T >200(250) GeV. Figure 2 shows the transverse mass distribution of the $W \rightarrow e\nu$ candidates.

Candidates for the process $Z \rightarrow e^+e^-$ are required to have two tight electrons, each with $E_T > 25$ GeV in the CC. The invariant mass of the dielectron pair is required to satisfy 60 GeV $< m_{ee} <$ 120 GeV. A total of 1997 Z boson candidates is selected. Figure 3 shows the invariant mass distribution of the $Z \rightarrow e^+e^-$ candidates.

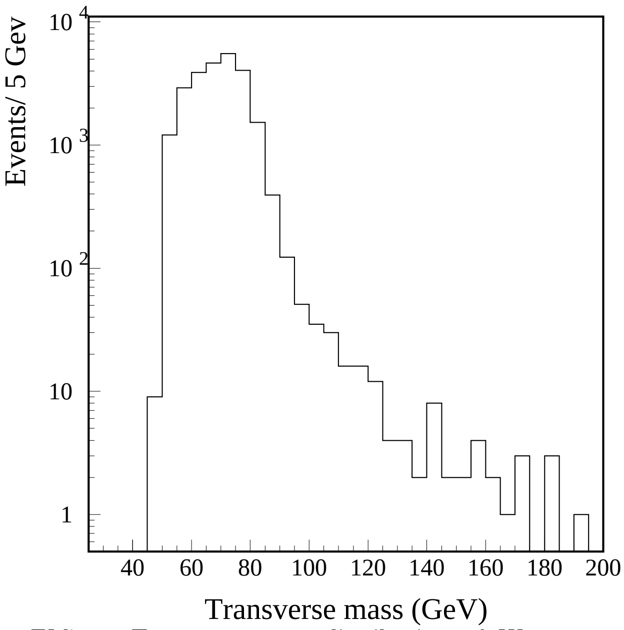

FIG. 2. Transverse mass distribution of $W \rightarrow e\nu$ event candidates.

IV. ANALYSIS PROCEDURE

In this section, we describe the Monte Carlo simulation program used to model the transverse mass spectrum. The background from the dominant processes that can mimic the $W \rightarrow e\nu$ signal is also estimated. We compare the data with the expectation from the Monte Carlo simulation and extract the decay width of the W boson using log-likelihood fits to the W boson transverse mass distribution.

A. Monte Carlo Simulation

The transverse mass spectrum for the W boson is modeled in three steps: W boson production, W boson decay, and a parameterized detector simulation [15,34,35].

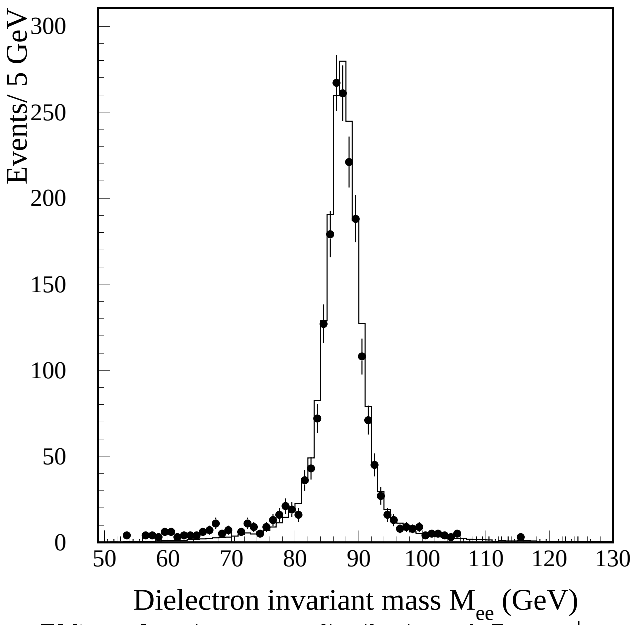

FIG. 3. Invariant mass distribution of $Z \to e^+e^-$ events compared to Monte Carlo simulation. The histrogram is the MC and the black dot with error bar is the data. The $Z \to e^+e^-$ candidate require both electrons be in the CC.

We first simulate the production of the W boson by generating its four momentum and other event characteristics, such as the z-position of the interaction vertex and the run luminosity. The luminosity is used to parameterize luminosity-dependent effects. To lowest-order, the mass of the W boson follows the Breit-Wigner distribution:

$$\sigma(Q) = \mathcal{L}_{q\bar{q}}(Q)\frac{Q^2}{(Q^2 - M_W^2)^2 + Q^4\Gamma_W^2/M_W^2}. \quad (6)$$

where Q is the invariant mass of W boson, M_W is the pole mass and Γ_W the decay width of the W boson, and $\mathcal{L}_{q\bar{q}}(Q)$ is called the parton luminosity. To evaluate $\mathcal{L}_{q\bar{q}}(Q)$, we generate $W \to e\nu$ events using the leading-order RESBOS [36] event generator and the different PDF models described in Refs. [37,38], and then select the events using the same kinematic and fiducial constrains as for the W and Z boson data samples. The resulting event distribution is proportional to the parton luminosity, which we parameterize with the function [39]:

$$\mathcal{L}_{q\bar{q}}(Q) = \frac{e^{-\beta Q}}{Q}. \quad (7)$$

where β is obtained from a fit of the MC events to Eq. 6.

The decay of the W boson is simulated in the MC and used to calculate the transverse momentum of the electron and other decay products. Any radiation from the decay electron or from the W boson can bias the measurement and has to be taken into account. $W \to \tau\nu \to e\nu\bar{\nu}\bar{\nu}$ events are indistinguishable from $W \to e\nu$ and are also included in the model, using a branching ratio of $Br(\tau \to e\nu\bar{\nu})/[1 + Br(\tau \to e\nu\bar{\nu})] = 0.151$.

Finally, we apply a parameterized detector simulation to the momenta of all decay products to simulate any observed recoil jets and electron momenta. The parameters giving the electron and recoil system response of the detector are fixed using data, which include Z bosons and their recoil jets, to study calorimeter response and resolution. The response to jets and electrons is parameterized as a function of energy and angle. Also included in the detector parameterization are effects due to the longitudinal spread of the interaction vertex and the luminosity-dependent response of the detector caused by multiple collisions.

Uncertainties in the input parameters to the MC will eventually limit the accuracy of the width measurement of the W boson. To study the uncertainties, we allow these input parameters to vary by one standard deviation and re-generate the corresponding transverse mass spectrum. We then fit it with a nominal MC template. If the positive and negative variations of the width of the W boson with respect to a parameter are not symmetric, the larger value is used for the uncertainty. This estimation is used to estimate the impact of the electron energy resolution, hadronic energy resolution, electron energy scale, hadronic energy scale, dependence on the W boson mass, electron angular calibration, and radiative corrections. Detailed studies of these parameters can be found in Ref. [15]. The uncertainties on Γ_W from the electron energy resolution and scale are 27 MeV and 41 MeV, respectively. The uncertainties from the hadronic energy resolution and scale lead to variations in Γ_W of 55 MeV and 22 MeV, respectively. The error on the W boson mass of 37 MeV has an effect of 15 MeV on Γ_W. The uncertainties from radiative decay and electron angular calibration correspond to 10 MeV and 9 MeV, respectively.

Uncertainties on Γ_W also arise from uncertainties in the production model and the parton distribution functions (PDFs). The uncertainty from the former is determined from the upper and lower limits [37] of the most uncertain parameter in the model. This leads to an uncertainty of 28 MeV due to parton luminosity and 12 MeV due to uncertainty in the transverse momentum of the W boson in the model. There are several PDF models currently in use. The uncertainty due to variation in PDFs is determined by using different PDFs, including MRSA [40], CTEQ4M and CTEQ5M [41], and finding the largest excursion from the value of Γ_W determined using the MRST PDF set [42], leading to a variation of 27 MeV. The value quoted for Γ_W is determined using the MRST PDFs. We chose MRST so that the results can be consistent with DØ mass analysis [15].

B. Backgrounds

Backgrounds to $W \to e\nu$ can affect the shape of the m_T spectrum and skew the measurement of Γ_W. We account for this by estimating the background as a function of m_T and adding this to the m_T distribution of the W boson from the Monte Carlo. The three dominant background sources are multijet events, $Z \to ee$, and $W \to \tau\nu$ decay products. The following describes how the backgrounds are estimated [28].

A large potential source of background is due to multijet events in which one jet is misidentified as an electron and the energy in the event is mismeasured, thereby yielding large $\not{E}_T$. This background is estimated using jet events from data, following the procedure called the "matrix method," described in Ref. [25,28,32]. The method uses two sets of data, each containing both signal and background. The first data set corresponds to the W data sample in this analysis. The second set contains a different mix of signal and background which is obtained with loose electron criteria (described in Sec. III A). We summarize below the essence of this method used to estimate the multijet background.

The number of multijet background (N^W_{BG}) events in the tight electron W data sample is given by

$$N^W_{BG} = \epsilon_j \frac{\epsilon_s N_l - N_t}{\epsilon_s - \epsilon_j}. \tag{8}$$

where N_l and N_t are the number of events in the W boson samples satisfying loose and tight electron criteria, respectively. The tight electron efficiency, ϵ_s, is the fraction of loose electrons that pass tight electron criteria, as determined by the Z boson sample, where one electron is required to pass the tight selection criteria and the other serves as an unbiased probe for determining relative efficiencies. The electron efficiency is obtained to be $\epsilon_s = (86.3 \pm 1.2)\%$. The jet efficiency ϵ_j is the fraction of loose "electrons" found in multijet events that also pass tight electron criteria. This sample is required to have $\not{E}_T \leq 15$ GeV to minimize the number of W bosons contained in it. The results is $\epsilon_j = (5.83 \pm 0.25)\%$. Once ϵ_s and ϵ_j are determined, we can extract the background-event distribution. The "electron" and "neutrino" transverse momenta and energies are used to form the transverse mass, and this distribution is shown in Figure 4. The total multijet background is estimated to be 368 ± 32 events in the region $m_T < 200$ GeV, with 25.4 ± 2.2 events in the range 90 GeV $< m_T <$ 200 GeV.

The background sample is smoothed in the region 85 GeV $< m_T <$ 200 GeV. We fit the distribution to an exponential function of the form $f_{BG} = \exp(a_0 + a_1 x + a_2 x^2 + a_3 x^3)$. The fitting parameters a_0, a_1, a_2 and a_3 [43] are used to generate the background distribution for the fit to the signal. For bins outside the fitted region, we use the original data itself, as shown in Figure 4.

Another source of background is due to $Z \to ee$ events in which one electron is undetected. This results in a momentum imbalance, with the event now being topologically indistinguishable from $W \to e\nu$ events. This background is also estimated using Monte Carlo events. The number of such Z boson events present in the W boson sample is calculated by applying the W boson selection criteria to MC $Z \to ee$ events generated using HERWIG [44] and processed through a GEANT [45] based simulation of the DØ detector, and then overlaid with events from random $p\overline{p}$ crossings. This is done to simulate the effect of the luminosity on the underlying event. Out of a total of 8870 $Z \to ee$ events, 48 pass the W boson event selection. Normalizing the Monte Carlo sample to the size of the data sample for equivalent luminosity, we estimate that there are 102 $Z \to ee$ events in the data sample.

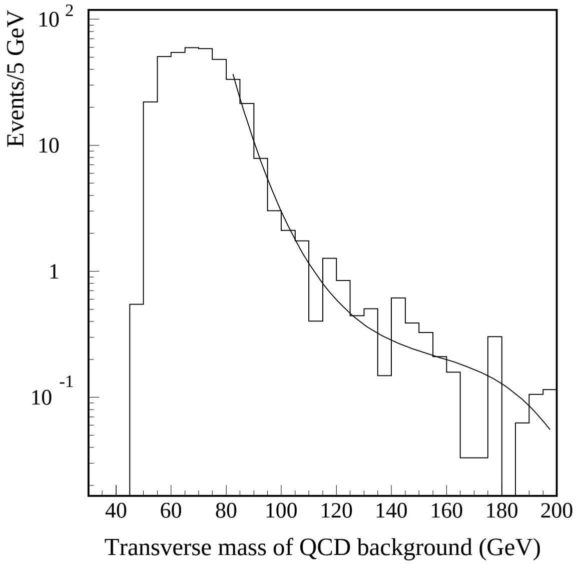

FIG. 4. The transverse mass distribution for the multijet background. The line represents the results of the fit described in the text.

$W \to \tau\nu$ events in which the τ decays into an electron and two neutrinos are indistinguishable from $W \to e\nu$ events on an event-by-event basis. Because τ undergoes a three-body decay, leading to a softer electron relative to $W \to e\nu$ events, the acceptance is reduced greatly by the standard E_T selection criteria. The size of this background is small, and it tends to add events with low values of m_T. This background is determined using the $W \to e\nu$ Monte Carlo, modified to include the decay of the τ lepton. The events are then passed through the same detector simulation used to model the $W \to e\nu$ signal.

The shape and total amount of background affect the fit used to determine the width of W boson. To estimate the uncertainty in Γ_W due to the uncertainty in absolute background, we scale up (and down) the fitted number of background events by an amount that corresponds to the total uncertainty in the background. This gives an uncertainty of 15 MeV for Γ_W extracted from the region 90 GeV $< m_T <$ 200 GeV. To estimate the uncertainty in Γ_W from the uncertainty in the shape of the background spectrum, we perform an ensemble study in which background is generated using a multinomial distribution. The multinomial distribution is defined by:

$$P(N_1, N_2, \ldots, N_{ch}) = N_{\text{total}} \prod_{i=1}^{ch} \frac{p_i^{N_i}}{N_i!}. \qquad (9)$$

where N_{total} is the total number of background events, ch is the number of the bins, p_i is the original distribution, and N_i is numbers of events in i-th bin. The total background N_{total} is kept at its central value, while the number of background events in each bin is allowed to fluctuate. The W boson width is then recalculated with the new background distribution. The variation in Γ_W is taken as the uncertainty. We found that this is 39 MeV for the fitted region of m_T.

C. Likelihood Fitting

We generate a set of Monte Carlo m_T templates with Γ_W varying from 1.55 GeV to 2.75 GeV at intervals of 50 MeV. These templates are normalized to the number of events in the region of $m_T <$ 200 GeV. The background distributions of multijet and $Z \to ee$ events are added to the templates and a binned likelihood is calculated for data. The m_T bin size is 5 GeV. The fitting region is chosen to be 90 GeV $< m_T <$ 200 GeV to minimize the systematic uncertainty. From the dependence of the likelihood on Γ_W, we obtain the W boson width and its error as: $\Gamma_W = 2.23^{+0.15}_{-0.14}$(stat.) GeV. The combined uncertainty, taking the statistical and systematic uncertainties contribution in quadrature, yields the result $\Gamma_W = 2.23^{+0.15}_{-0.14}$(stat.) $\pm$ 0.10(sys.) GeV$= 2.23^{+0.18}_{-0.17}$ GeV. The χ^2 for the best fit is an acceptable 25.9 for 22 degrees of freedom, corresponding to a probability of 26%. A comparison of the observed spectrum to the probability density function in the fitting region through a Kolmogorov-Smirnov test, which compares the observed cumulative distribution function for a variable with a specified theoretical distribution, yields $\kappa = 0.434$, which is evidence of a good fit.

Figure 5 shows a fit to the likelihood, which corresponds to a fourth-order polynomial fit that determines the peak position. Figure 6 shows the m_T spectrum for the data, the normalized MC sample, and the background.

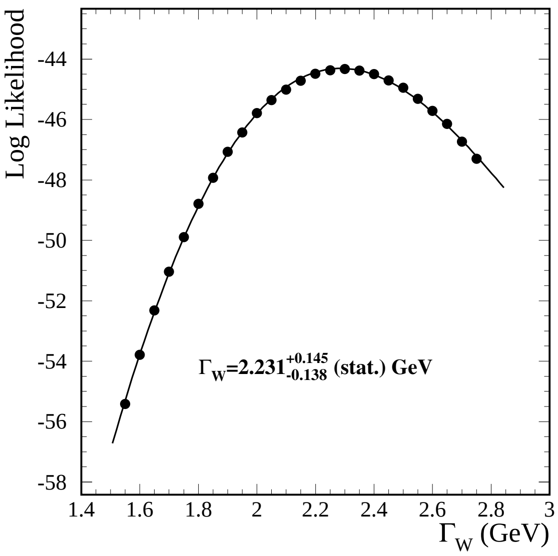

FIG. 5. Results of the log-likelihood fit of the data to Monte Carlo templates for different Γ_W.

As a consistency check of the fitting method, we also determine the W boson width from the ratio of the number of events in the fitting region of 90 GeV $\leq m_T \leq$ 200 GeV to the number of events in the entire spectrum. This yields $\Gamma_W = 2.22 \pm 0.14$(stat.) GeV, compared to $\Gamma_W = 2.23^{+0.15}_{-0.14}$(stat.) GeV for the independent maximum likelihood fit in the same region. All results show good agreement.

Sources of systematic uncertainties in the determination of the W boson width are those that can affect the shape of the transverse mass distribution. These include the uncertainties from input parameters to the MC program and from background estimation. Details can be found in Ref. [28]. Table I lists all the sources of systematic uncertainty for the decay width of the W boson.

Comparing to the SM prediction of $\Gamma(W) = 2.0921 \pm 0.0025$ GeV, we find the difference between SM prediction and our meaasurement to be $0.24^{+0.18}_{-0.17}$ GeV, which is the width for the W boson to decay into final states other than the two lightest quark doublets and the three lepton doublets. We set a 95% confidence level upper limit on the W boson width to non-SM final states. Assuming the uncertainty is Gaussian, we set a 95% confidence level upper limit on the invisible partial width of the W

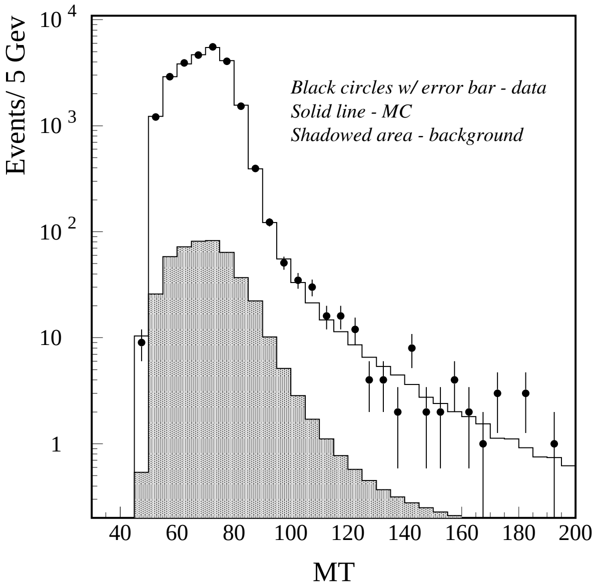

FIG. 6. Comparison of data to the Monte Carlo templates for the best fit. The black circles with error bars are the data. The solid line of the histogram corresponds to the MC templates with $\Gamma(W) = 2.23$ GeV normalized to the expected number of W boson events. The shadowed area is the background.

Source	$\delta\Gamma_W$(MeV)
Hadronic energy resolution	55
EM energy scale	41
Background ensemble studies	39
Luminosity slope dependence	28
EM energy resolution	27
PDF	27
Hadronic energy scale	22
Background normalization	15
W boson mass	15
Production model	12
Radiative correction	10
Selection bias	10
Angular calibration of e trajectory	9
Total systematic uncertainty	99
Total statistical uncertainty	+145 −138
Total uncertainty	+176 −170

TABLE I. Systematic uncertainties and the total uncertainty on the W boson width measurement.

boson to be 0.59 GeV. Under the assumption that there is no correlation between indirect measurement and direct measurement of the W boson decay width and within the framework of SM, we can combine both analysis and obtain $\Gamma_W = 2.162 \pm 0.062$ GeV. The 95% confidence level upper limit on the invisible partial width of the W boson is 0.191 GeV.

V. CONCLUSIONS

We have directly measured the decay width of the W boson by fitting the transverse mass in $W \to e\nu$ events in $p\bar{p}$ collisions at 1.8 TeV, and obtain:

$$\Gamma_W = 2.23^{+0.15}_{-0.14}(\text{stat.}) \pm 0.10(\text{syst.})\ \text{GeV} \quad (10)$$

$$= 2.23^{+0.18}_{-0.17}\ \text{GeV}. \quad (11)$$

This result is consistent with the prediction of the standard model.

VI. ACKNOWLEDGMENTS

We thank the staffs at Fermilab and collaborating institutions, and acknowledge support from the Department of Energy and National Science Foundation (USA), Commissariat à L'Energie Atomique and CNRS/Institut National de Physique Nucléaire et de Physique des Particules (France), Ministry for Science and Technology and Ministry for Atomic Energy (Russia), CAPES and CNPq (Brazil), Departments of Atomic Energy and Science and Education (India), Colciencias (Colombia), CONACyT (Mexico), Ministry of Education and KOSEF (Korea), CONICET and UBACyT (Argentina), The Foundation for Fundamental Research on Matter (The Netherlands), PPARC (United Kingdom), Ministry of Education (Czech Republic), A.P. Sloan Foundation, NATO, and the Research Corporation.

* Also at University of Zurich, Zurich, Switzerland.
† Also at Institute of Nuclear Physics, Krakow, Poland.

[1] S. Glashow, Nucl. Phys. **22**, 579 (1961).
[2] S. Weinberg, Phys. Rev. Lett. **19**, 1264 (1967) .
[3] A. Salam in *Elementary Particle Theory*, edited by N. Svartholm (Almquist and Wiksells, Stockholm, 1969), 367.
[4] W. Bardeen, H. Fritzsch, M. Gell-Mann in *Scale and Conformal Symmetry in Hadron Physics*, edited by R. Gatto (Wiley, New York, 1973), 139.
[5] D. Gross and F. Wilczek, Phys. Rev. D **8**, 3633 (1973).
[6] S. Weinberg, Phys. Rev. Lett. **31**, 494 (1973).
[7] UA1 Collaboration, G. Arnison *et al.*, Phys. Lett. B **122**, 103 (1983).
[8] UA2 Collaboration, P. Bagnaia *et al.*, Phys. Lett. B **122**, 476 (1983).
[9] UA1 Collaboration, G. Arnison *et al.*, Phys. Lett. B **126**, 398 (1983).

[10] UA2 Collaboration, P. Bagnaia *et al.*, Phys. Lett. B **129**, 130 (1983).
[11] D. E. Groom *et al.*, Eur. Phys. J. C **15**, 1-878 (2000).
[12] J. Rosner, M. Worah, and T. Takeuchi, Phys. Rev. D **49**, 1363 (1994).
[13] R. M. Barnett *et al.*, Phys. Rev. D **54**, 1 (1996).
[14] CDF Collaboration, F. Abe *et al.*, Phys. Rev. D**43**, 2070 (1991).
[15] DØ Collaboration, B. Abbott *et al.*, Phys. Rev. D **58**, 092003 (1998).
[16] L3 Collaboration, M. Acciarri *et al.*, Phys. Lett. B **413**, 176 (1997).
[17] ALEPH Collaboration, R. Barate *et al.*, Phys. lett. B **422**, 384 (1998).
[18] OPAL Collaboration, K. Ackerstaff *et al.*, Eur. Phys. J. C **1**, 395 (1998).
[19] Delphi Collaboration, P. Abreu *et al.*, Eur. Phys. J. C **2**, 581 (1998).
[20] A. D. Martin, R. G. Roberts and W. J. Stirling, Phys. Lett. B **306**, 147 (1993) and **309**, 492 (1993).
[21] LEP Electroweak Working Group, CERN Report No. CERN-EP-2001-098, hep-ex/0112021.
[22] UA1 Collaboration, C. Albajar *et al.*, Phys. Lett. B **253**, 503 (1991).
[23] UA2 Collaboration, J. Alitti *et al.*, Phys. Lett. B **276**, 365 (1992).
[24] CDF Collaboration, F. Abe *et al.*, Phys. Rev. D **52**, 2624 (1995).
[25] DØ Collaboration, B. Abbott *et al.*, Phys. Rev. D **61**, 072001 (2000).
[26] V. D. Barger and R. J. N. Phillips, in *Collider Physics*, Volume 71 of Frontiers in Physics (Addison-Wesley, 1987).
[27] CDF Collaboration, F. Abe *et al.*, Phys. Rev. Lett. **85**, 3347 (2000). CDF measured the W boson width in both the $e\nu$ and $\mu\nu$ channels. The number reported is their combined result.
[28] Qichun Xu, Ph. D. Thesis, the University of Michigan, 2001 (unpublished). *http://wwwd0.fnal.gov/results/publications_talks/thesis/xu/qichun_thesis.html*.
[29] The origin of the coordinate system is the reconstructed position of $p\bar{p}$ interaction when describing the interaction, and the geometrical center of the detector when describing the detector. It refers to the detector here.
[30] DØ Collaboration, S. Abachi *et al.*, Nucl. Instr. and Methods in Phys. Res. A **338**, 185 (1994).
[31] DØ Collaboration, B. Abbott *et al.*, Phys. Rev. D **58**, 052001 (1998).
[32] DØ Collaboration, V. M. Abazov *et al.*, Phys. Lett. B 513, 292 (2001).
[33] DØ Collaboration, S. Abachi *et al.*, Phys. Rev. D **52**, 4877 (1995).
[34] Eric M. Flattum, Ph. D. Thesis, Michigan State University, 1996 (unpublished), *http://wwwd0.fnal.gov/results/publications_talks/thesis/flattum/eric_thesis.html*.
[35] Ian Malcolm Adam, Ph. D. Thesis, Columbia University, 1997 (unpublished), *http://wwwd0.fnal.gov/results/publications_talks/thesis/adam/ian_thesis_all.html*.
[36] C. Balazs and C. P. Yuan, Phys. Rev. D **56**, 5558 (1997).
[37] G. A. Ladinsky and C. P. Yuan, Phys. Rev. D **50**, 4239 (1994).
[38] P. B. Arnold and M.H. Reno, Nucl. Phys. **B319**, 37 (1989); **B330**, 284E (1990); R. J. Gonsalves, J. Pawlowski, and C-F. Wai, Phys. Rev. D **40**, 2245 (1989).
[39] DØ Collaboration, S. Abachi *et al.*, Phys. Rev. Lett. **77**, 3309 (1996); DØ Collaboration, B. Abbott *et al.*, Phys. Rev. D **58**, 012002 (1998).
[40] A. D. Martin, W. J. Stirling, R. G. Roberts, Phys. Lett. B **354**, 155 (1995).
[41] The Coordinated Theoretical-Experimental Project on QCD, *http://www.phys.psu.edu/cteq*.
[42] A. D. Martin, R. G. Roberts and W. J. Stirling, R. R. Thorne, hep-ph/0110215.
[43] We found the fitting parameters as $a_0 = (3.9153 \pm 0.0012) \times 10^1$, $a_1 = (-7.5100 \pm 0.0044) \times 10^{-1}$, $a_2 = (4.7087 \pm 0.0041) \times 10^{-3}$ and $a_3 = (-1.00461 \pm 0.00095) \times 10^{-5}$.
[44] G. Marchesini *et al.*, Comput. Phys. Commun. **67**, 465 (1992).
[45] F. Carminati *et al.*, GEANT *Users Guide*, CERN Program Library W5013, 1991 (unpublished).